Tariq Abuhamdia
Virginia Polytechnic Institute and State University

Jacob Rosen*
University of California at Santa Cruz

Constant Visual and Haptic Time Delays in Simulated Bilateral Teleoperation: Quantifying the Human Operator Performance

Abstract

Visual feedback and force feedback (haptics) are the two streams of information in a robotic bilateral teleoperation where the operator manipulates a robot in a remote location. Delivering the visual and the haptic information depends in part on the characteristics of the communication network and results in a nonsynchronized delay. The goal is to study the effect of constant nonsynchronized and synchronized time delay of visual and haptic information on the human teleoperation performance. The experimental setup included a virtual reality environment, which allows the operator to manipulate the virtual objects in a simulated remote environment through a haptic device that renders the force feedback. The visual and the haptic information were delayed independently in the range of 0–500 ms, creating 121 different scenarios of synchronized and nonsynchronized delays. Selecting specific parameters of the remote virtual environment guaranteed stable teleportation, given the time delays under study. The experimental tasks included tracing predefined geometrical shapes and a pick-and-place task, which simulates both structured and unstructured interactions under the influence of guiding forces. Eight subjects ($n = 8$) participated in the experiment performing three repetitions of three different teleoperation tasks with 121 combinations of visual and haptic time delays. The measured parameters that were used to assess the human performance were the task completion time and the position errors expressed as a function of the visual and the haptic time delay. Then, regression and ANOVA analyses were performed. The results indicated that the human performance is a function of the sum of the two delays. As the sum of the two delays increases, the human performance degrades and is expressed with an increase in completion time and position errors. The performance degradation is more pronounced in the pick-and-place task compared to the tracing task. In scenarios where the visual and the haptics information were out of synchronization, the human performance was better than intentionally delaying one source of information in an attempt to synchronize and unify the two delays. The results of this study may be applied to any teleoperation tasks over a network with inherent time delays and more specifically to telesurgery in which performance degradation due to time delay has a profound effect on the quality of the healthcare delivered, patient safety, and ultimately the outcomes of the surgical procedure itself.

Presence, *Vol. 22, No. 4, Fall 2013,* 271–290
doi:10.1162/PRES_a_00158

*Correspondence to rosen@ucsc.edu.

1 Introduction

Sensory information perceived by the human senses is critical to successful human interaction with the external environment. Once a teleoperating system is introduced as a mediating layer between the human operator and a remote environment, it may simultaneously enhance and degrade different inputs and outputs generated by the human operator and in that way affect the human performance. From one perspective, the teleoperation system may enhance human vision by allowing the operator to watch the remote site using various wavelengths (infrared, ultrasonic, etc.) that cannot be sensed by the human eye. Moreover, the teleoperating system may scale down or up human arm movements along with filtering hand tremor; in that way it may provide better dexterous control and manipulation of the object located at the remote site. From another perspective, the teleoperation system may also degrade the human performance by limiting the sensory information in terms of type, bandwidth, and synchronization due to inherent time delays in the communication system between the operator console and the remote manipulator. For the purpose of studying, simulating, and training, teleoperation systems, the remote environment, along with the remote robotic system, may be completely or partly replaced by a virtual environment in a way that provides better control of the internal and external tested variables such as nonsynchronized time delays of various sensory input channels.

The delay of systems' response to an input or perturbation is a common and inherent phenomenon in physical, natural, and manmade systems. The systems' delay in the time domain may be translated to the frequency domain and expressed by a limited bandwidth of the system's response.

Dedicated communication lines are becoming cheaper and affordable; nevertheless, the speed in which information can travel in any line is bounded by the speed of light. Even under the best case scenario of remote teleoperation, in which the information is traveling at the speed of light, time delay will always be an integral part of the process and affect the operator's performance.

Time delay in the communication network affects human performance during a teleoperation task, especially when visual and haptic feedback is involved. The human performance degradation as a function of visual or force feedback was mainly studied individually. However, their combined effect with different combinations of time delays was not studied extensively. Haptic and visual feedback are subject to different technological barriers. Haptic feedback time delay is dictated by the shear bandwidth of the network; however, visual time delay depends on computational and algorithmic power effecting the time required to compress and decompress the video signal. Given the stochastic nature of networks, the network time delay is also a function of the communication traffic; therefore, it may be represented by a distribution and not necessarily by a fixed value (Sankaranarayanan & Hannaford, 2008).

Pioneering research efforts studying the effect of visual time delay using an experimental approach indicated that the teleoperated task performance is degraded as a function of time delay (Sheridan & Ferrell, 1963; Ferrell, 1965). It was shown experimentally that the completion time of a teleoperated task was reduced significantly when visual predictors were used in telerepositioning tasks compared to cases where visual predictors were not used (Kelley, 1968; Hashimoto, Sheridan, & Noyes, 1986).

Based on early research efforts, it was recommended that during teleoperation under time delays, force should not be continuously fed back into the operator's hand while holding the controller in order to maintain and guarantee the stability of the system (Ferrell, 1965). Given visual feedback, the operator may ignore the disturbance expressed as the delayed force feedback signal, and avoid potential system instability by adopting a move-and-wait strategy or by utilizing supervisory control. Several alternative approaches were proposed to cope with the time-delayed force feedback including: (1) bandwidth reduction (Vertut, Micaelli, Marchal, & Guttet, 1981), (2) converting the force feedback into a visual input, (3) providing force feedback to the operator's other hand, and (4) predicting the force feedback to compensate for the delay (Sheridan, 1992).

A recent research effort studied the effect of force feedback (haptic) and visual feedback delays on the human performance under three scenarios: (1) haptic input delay, (2) visual input delay, and (3) haptic and visual inputs that are equally and simultaneously delayed (Jay and Hubbold, 2005). A reciprocal tapping task was selected, and the subject performance was quantified by three parameters: (1) target missing times, (2) intertap interval (ms), and (3) mean difficulty rating. The study concludes that time delays of both visual and haptic inputs degrade human performance. Moreover, the time delay of the haptic input has more significant effect in terms of human performance degradation than the time delay of the visual input. However, delaying both inputs simultaneously led to the most significant degradation in human performance. This study maps only three discreet points in a limited range of 0–150 ms out of many operation points defined by a combination of time delays in vision and haptics. In realistic teleoperation conditions, the system operator will experience unequal time delays and the larger spectrum in these two channels, given the nature of the signals and preprocessing and postprocessing algorithms that need to be applied.

This study was inspired by a series of field experiments emulating realistic telesurgery scenarios, in which a surgical robot (Raven; Sankaranarayanan et al., 2007) was teleoperated using wired and wireless networks under a wide spectrum of time delays (Lum, Friedman, King, Donlin, Sankaranarayanan et al., 2007; Lum, Rosen et al., 2007; Lum et al., 2008; Rosen, Brown, Chang, Sinanan, & Hannaford, 2006; Rosen, Lum, Sinanan, & Hannaford, 2011). The results of these preliminary studies indicated human performance degradation as the time delays increased. However, given their nature as field experiments, time delay was not a controlled variable. The goal of this study is to provide quantitative measures of the human performance degradation in bilateral teleoperation tasks as a function of fixed visual time delay and fixed haptic time delay, as two independent and controlled variables, while performing tracing and object manipulation tasks.

2 Methodology

2.1 Time Delay in Bilateral Teleoperation

2.1.1 Multi-Loop Multi-Delay System. Time delay is inherent in any teleoperating system and is introduced in several locations of the bilateral input-output pathway scheme (Figure 1). The input command signal is delayed in the input pathway while both the haptic and the visual feedback signals are delayed in the feedback pathways. Figure 1 depicts the general scheme for a bilateral teleoperator with input and output pathways where D_{I} is the input time delay, $D_{\mathrm{f.h}}$ is the haptic feedback time delay, $D_{\mathrm{f.v}}$ is the visual feedback time delay, and *PRP* is the psychological refractory period. Three control loops can be identified: the haptic loop (paths 0, 1, 2 and 4), the visual (paths 0, 1, 3 and 5), and the internal human control loop (paths 0 and 4). The PRP is defined as a constant time delay of 300 ms (Salvandy, 1987), and is considered part of path 0.

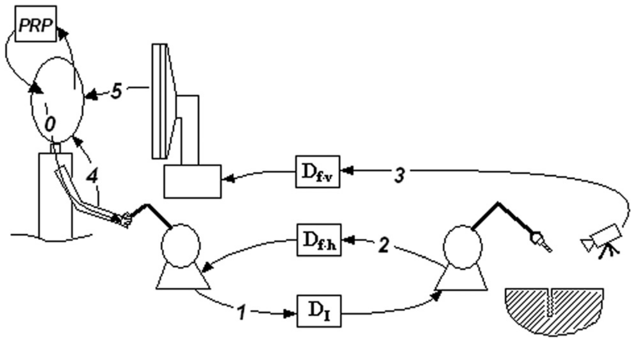

Figure 1. *General scheme for bilateral teleoperator depicting the various pathways of information and the corresponding time delays along each communication channel.*

Human operator performance during teleoperation is affected by the time delays in all the pathway loops. The closed loop visual time delay in the system is expressed as $D_{\mathrm{V}} = D_{\mathrm{I}} + D_{\mathrm{f.v}}$, and the closed loop haptic delay is expressed as $D_{\mathrm{H}} = D_{\mathrm{I}} + D_{\mathrm{f.h}}$. The domain of the time delay defined by D_{V} and D_{H} can be divided into two distinct regions as shown in Figure 2. If the visual time delay is greater than the haptic time delay, namely $D_{\mathrm{V}} > D_{\mathrm{H}}$, then the operator first feels the haptic feedback and sees the visual feedback later; hence, this region is referred to as the feel-first-see-later region. If the haptic time delay is greater than the visual time delay, namely $D_{\mathrm{H}} > D_{\mathrm{V}}$, the operator sees the visual feedback first and feels the haptic feedback later; consequently, this region may be referred to as the see-first-feel-later region. Along the diagonal line which defines the boundary between

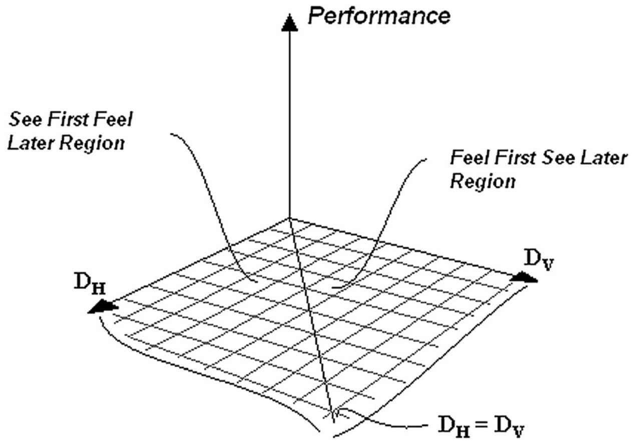

Figure 2. *The delay domain divided into two main regions: "see-first-feel-later" ($D_H > D_V$), and "feel-first-see-later" ($D_H < D_V$). Along the boundary between these two regions $D_H = D_V$.*

these two regions, the visual and the haptic time delays are equal, $D_H = D_V$; as a result, the visual and the force feedback information are perceived by the human operator at the same time. The human performance may be measured along the vertical axis for every pair of time delays (D_H, D_V) given the various performance indexes to obtain a performance surface.

2.1.2 The Experiment Setup: Bilateral Teleoperator Simulator. A simulated bilateral teleoperation with a real master device (PHANToM Omni, SensAble, Inc.) and a virtual slave in haptic virtual environment (VR) comprised the experimental setup. The operator controls the simulated environment by manipulating the master device, which is capable of rendering haptic feedback while the remote environment is displayed on a screen. This experimental setup provides full control over the haptic and the visual time delays; thus, the setup allows the researcher to set the desired value for each variable independently. The experimental setup is illustrated in Figure 3(b).

The stability analysis of the experimental system is done based on the two-port hybrid matrix model and the forward flow network architecture (Hannaford, 1989). Figure 4(a) depicts a modified two-port network and Figure 4(b) illustrates the forward flow architecture, where F is the force, Z is the mechanical impedance, V is the velocity, D_I is the input time delay, and $D_{f.h}$ is the haptic feedback time delay.

The subscript m denotes master, s slave, h human, e environment, and d desired. The two-port network and the bilateral forward flow network shown in Figures 4(a) and 4(b) are used to derive the hybrid matrix $h(t)$ which relates the output vector $[F_h \quad V_e]^T$ to the input vector $[V_m \quad F_e]^T$ as

$$\begin{bmatrix} F_h \\ V_e \end{bmatrix} = \begin{bmatrix} h_{11} & h_{12} \\ h_{21} & h_{22} \end{bmatrix} \begin{bmatrix} V_m \\ F_e \end{bmatrix}. \tag{1}$$

The individual elements of the hybrid matrix $h(t)$ in Equation 1 are defined by applying the superposition principle to the network in Figure 4(b) and the result is given by

$$h = \begin{bmatrix} \left.\frac{F_h}{V_m}\right|_{F_e=0} & \left.\frac{F_h}{F_e}\right|_{V_m=0} \\ \left.\frac{V_e}{V_m}\right|_{F_e=0} & \left.\frac{V_e}{F_e}\right|_{V_m=0} \end{bmatrix}. \tag{2}$$

Explicitly expressing the elements of matrix h and transforming them to the frequency domain yields the matrix $H(s)$ as

$$H(s) = \begin{bmatrix} Z_m & e^{-sD_{f.h}} \\ e^{-sD_I} & \frac{1}{Z_s+Z_e} \end{bmatrix}. \tag{3}$$

Assuming that all the initial conditions are zero (Hannaford, 1989), and for an LTI network, Z_m, Z_s, and Z_e are defined in the frequency domain as

$$Z_m = M_1.s + b_1 + \frac{k_1}{s}, \tag{4}$$

$$Z_s + Z_e = M_2.s + b_2 + \frac{k_2}{s}, \tag{5}$$

where M_1 is the operator's arm inertia (the Omni manipulator's inertia was neglected because it is very small relative to the human arm's inertia), k_1 is the equivalent stiffness of the arm, and b_1 is the overall master side damping. Note that Z_s and Z_e are merged into single equivalent impedance; thus, M_2 is the inertia of the slave manipulator, k_2 is the stiffness of the virtual walls, and b_2 is the damping of the virtual environment. Using Equations 4 and 5, the matrix $H(s)$ > can be rewritten as

$$H(s) = \begin{bmatrix} M_1.s + b_1 + \frac{k_1}{s} & e^{-sD_{f.h}} \\ e^{-sD_I} & \frac{1}{M_2.s+b_2+\frac{k_2}{s}} \end{bmatrix}. \tag{6}$$

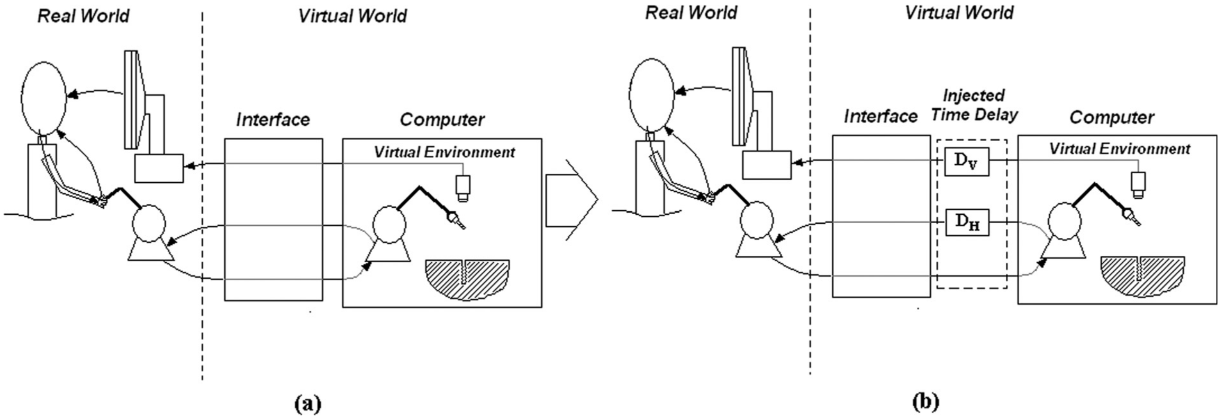

Figure 3. *A simulated bilateral teleoperation with a real master device (PHANToM Omni) and a virtual slave with a haptic VR. (a) a typical VR setup with no time delay, and (b) a VR setup with simulated time delays in the visual (D_V) and haptics (D_H) communication channels of the human interface.*

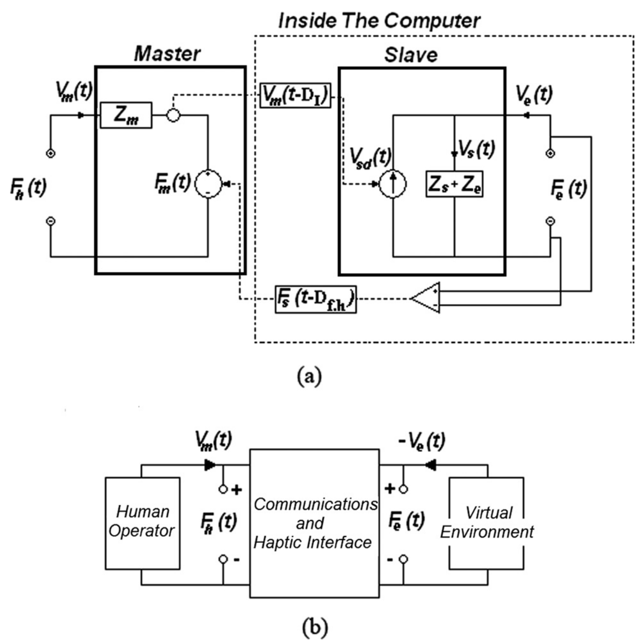

Figure 4. *Two-port network. (a) Schematic block diagram, and (b) bilateral forward flow network configuration.*

A sufficient condition for stable operation is a passive network. This can be tested using the scattering operator $S : L_2^n(R_+) \to L_2^n(R_+)$ that is defined by

$$F - V = S(F + V), \tag{7}$$

which maps effort plus flow, into effort minus flow (Magnusson et al., 1992). For LTI systems, the scattering operator S can be expressed in the frequency domain as

$$S(s) = \begin{bmatrix} 1 & 0 \\ 0 & -1 \end{bmatrix} (H(s) - I)(H(s) + I)^{-1}. \tag{8}$$

Substituting Equation 6 into Equation 8 results in

$$S(s) = \begin{bmatrix} \frac{(-1+Z_m)\left(1+\frac{1}{Z_s+Z_e}\right)}{e^{-sD_I}+(1+Z_m)\left(1+\frac{1}{Z_s+Z_e}\right)} & 0 \\ 0 & \frac{(1+Z_m)\left(-1+\frac{1}{Z_s+Z_e}\right)}{e^{-sD_{f.h}}+(1+Z_m)\left(1+\frac{1}{Z_s+Z_e}\right)} \end{bmatrix}. \tag{9}$$

If S is a bounded operator, its norm is defined by

$$\|S\| = \sup_{\omega} \|S(j\omega)\| = \sup_{\omega} \lambda^{1/2}(S^H(j\omega)S(j\omega)), \tag{10}$$

where λ is the eigenvalue of the matrix $S^H(j\omega)*S(j\omega)$, the asterisk "*" refers to matrix multiplications, and $S^H(j\omega)$ is the Hermetian of $S(j\omega)$. A system is passive if and only if the norm of its scattering operator is less than or equal to one. A proof can be found in Anderson and Spong (1989). Evaluating $\sup_{\omega} \lambda^{1/2}[S^*(j\omega)S(j\omega)]$ is straightforward from Equation 9.

Given the selected time delay range from 0 to 500 ms, a value for the damping coefficient b_1 was found such that the norm of S is bounded by a value of one for the impedances Z_e, Z_s, and Z_m, so the system remains passive within the tested range of time delays.

Table 1. *Summary of the Systems' Parameters*

Parameter	Value
M_1	0.3–3.5 kg
k_1	180–1000 N/m
M_2	0
b_2	0
k_2	50 N/m

The stiffness of the human shoulder was estimated in the range of 45–90 Nm/rad (Flash & Gurevich, 1997) while the equivalent stiffness at a hand located between 0.3 and 0.5 m away from the shoulder is in the range of 180–1000 N/m. The human arm mass varies between 0.3–3.5 kg during circular movements (Pfann, Corcos, Moore, & Hasan, 2002). Table 1 summarizes the simulator parameters used. M_2 and b_2 are set to zero. The weight of real objects of the same size as the manipulated virtual objects is very small compared to the human arm's inertia, so its effect can be neglected. Further, the damping force can be neglected in the remote virtual environment because it resembles friction force with room air. Moreover, we wanted to focus on the time delays' effect and reduce the effect of the environment physics as independent variable on the experiment. In this context, the assumptions are logical, and the resulting haptic interface remains significant and is similar to real haptic devices available commercially, including surgical devices. For these parameters, the problem can now be written as minimizing the norm of S given the following conditions:

$$\|S(j\omega)\| \leq 1, 0 \leq M_1 \leq 3.5\,\text{kg}, 0 \leq k_1 \leq 1000\,\text{N/m},$$
$$0 \leq k_2 \leq 50, M_2 = 0, b_2 = 0, \text{ and } 0 \leq D_H \leq 500\,\text{ms}. \tag{11}$$

Using a brute force numerical solution and solving Equation 11 for b_1 results in $b_1 = 5.5$ N·s/m. This value of damping coefficient may be varied as a function of the time delay. However, in order to minimize the experiment's variables, a single value of damping was used for the entire experimental protocol. The wave variable technique was also implemented and experimentally tested. Preliminary results indicated that transparency cannot be guaranteed to be similar across the entire range of the time delay under study. With wave variables, the nature of the reflected forces with high delays is affected; the reflected stiffness has different values; further, damping and inertial effects emerge as a function of time delay (Niemeyer, 1996). One consequence of utilizing wave variables was that uncontrolled variables were introduced to the experiment; consequently, wave variables were not used.

The master manipulator used in this experiment is a 6-degree-of-freedom PHANToM Omni (SensAble). The PHANToM Omni rendered force in three directions, X, Y, and Z. The virtual environment was developed in C++, run on a PC (Pentium IV, dual core 1.7 GHz processor with 1 GB RAM), and rendered graphically on a 21-in. monitor. The position and the force sampling rate was 1 kHz, and the picture refresh rate was 60 Hz.

2.2 Experimental Design

2.2.1 Hypothesis. The experimental design is based on two hypotheses (null hypothesis and alternative hypothesis) that will be statistically tested using ANOVA. The null hypothesis H_0 states that the two time delays (the visual time delay, D_V; and the haptics time delay, D_H) do not create any significant change of the human performance indexes. The alternative hypothesis (H_1) claims that the two time delays create significant change in all the human performance indexes ($p < .004$).

2.2.2 Experiment Tasks. The Society of American Gastrointestinal and Endoscopic Surgeons (SAGES), one of the major professional surgical organizations, has developed a curriculum for teaching minimally invasive surgical skills termed the Fundamentals of Laparoscopic Surgery (FLS) which includes both cognitive and psychomotor skills. The skills assessment consists of five tasks. The FLS skills tasks have been validated to show significant correlation between score and postgraduate year (Fried et al. 2004; Peters et al., 2004) and are considered by many to be the gold standard in minimally invasive surgical skill assessment. The block transfer (pick and place) task as well as cutting a piece of cloth along a circle are two of five tasks which define the FLS. As part of a parallel research effort aimed at developing objective algorithms for surgical skill assessment, it was shown that the majority of the surgical tasks can be decomposed using three archetypes including tissue manipulation (represented by the FLS block transfer), tissue dissection (represented by the FLS circle cutting), and suturing (represented by FLS suturing and knot tying; Brown, Rosen, Chang, Sinanan, & Hannaford, 2004; Harnett, Doarn, Rosen, Hannaford, & Broderick, 2008; Rosen et al., 2002; Rosen et al., 2003; Rosen et al., 2006). In addition, further deconstruction of surgical manipulation archetypes may lead to four independent unite actions (Oi) including: grasp/release an object ($O1$), translate an object along an arbitrary trajectory ($O2$), translate an object along a prescribed trajectory ($O3$), and ordinate an object ($O4$) (Slutski, 1998).

Using the FLS skill assessment tasks as the framework for the study, the two selected tasks included in the experimental protocol were: (1) tracing 2D geometrical shapes, and (2) a pick-and-place task. A square and a circle were chosen to be the 2D geometrical shapes for the tracing tasks, and a configuration of a 4×2 array of virtual spheres, which had to be relocated from their initial positions to new designated positions, was selected for the pick-and-place task. The selected tasks were performed in a 2D plane (XY plane). The third dimension (Z axis) was eliminated to avoid a depth illusion effect. These tasks represent a generalization of two of the FLS skill assessment tasks. Using the previously defined terminology, tracing 2D geometries is classified as an $O3$ task while the pick-and-place task is associated with the combination of $O1$ and $O2$.

A quantitative estimation of the geometrical shape complexity is defined by Equation 12 (Slutski, 1998). The geometrical shape complexity (C) depends on the number of curvilinear sections in the shape (V), the number of changes of the curvature sign (U), and the sum of absolute increment of the inclination angle (Φ), and it is defined by

$$C = U + V + \frac{\Phi}{\pi}. \qquad (12)$$

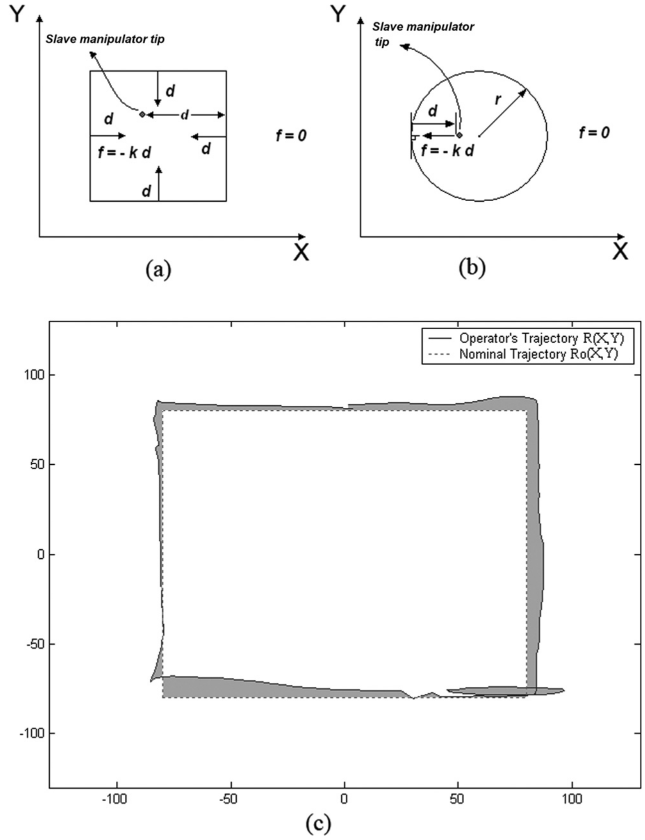

Figure 5. *The force field generated by the system as a feedback during the tracing tasks. (a) The square shape with Cartesian force field. (b) The circle shape with force field in a radial coordinate system. (c) A typical result of the square tracing experiment under visual and haptic time delay.*

2.2.3 Tracing Square and Circle of Elastic Boundaries.

Solid square and circle were presented to the subjects on a screen, one at a time, along with a small dot that represents the tip of the remote manipulator (slave). The subjects were asked to trace the boundaries of the presented shapes using the master manipulator as quickly and accurately as possible. A force field was rendered for the two shapes that was linearly proportional (Hook's law) to the penetrating distance into the shape boundaries as illustrated in Figure 5. The force generated by the field was set to be proportional to the penetration distance (d) into the shape's boundaries and zero outside the boundaries. Based on Equation 12, the configuration complexity for the square form is equal to

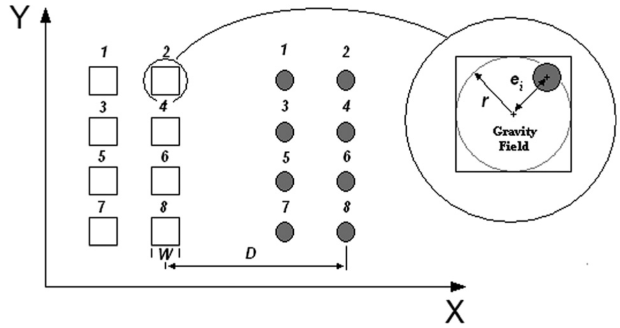

Figure 6. *The configuration of the pick-and-place task.*

($C = 0 + 0 + 2\pi/\pi = 2$) and for the circle is equal to ($C = 1 + 0 + 2\pi/\pi = 3$).

The tracing error is expressed by Equation 13, and a typical example is depicted in Figure 5. The force is set to be proportional to the penetration into the shape and zero elsewhere. The error is defined as the absolute area between the user's trajectory R and the nominal shape R_0 (Salvendy, 1987; Stanney, 2002).

$$E = \oint |f(R - R_0)|dR. \tag{13}$$

The nominal shape (dashed line) as well as the actual trajectory (solid line) generated by the subject are depicted in Figure 5(c); the tracing error as defined by Equation 13 is the shaded area between the two trajectories.

2.2.4 Pick-and-Place Task. The task consisted of moving eight spheres, arranged in a 4×2 array, one sphere at a time, from one location on the left to another designated location on the right as shown in Figure 6. The subject grasped the sphere by pressing a button located on the master manipulator, and released the sphere by releasing the button. Each sphere was numbered and must be relocated to match the target number. A margin (r) was defined around each target location. Releasing the sphere within the margins resulted in a successful transfer. If the sphere was released outside of the margin, the sphere was automatically moved back to its original location and the subject had to repeat the transfer. Each target had a linear force field with stiffness constant equal to k_2, which attracted the user to the center of the target.

The error e_i defining the accuracy error for the transfer of each sphere is defined as the distance between the target and the actual releasing location. The sum of the eight spheres' accuracy error was calculated to represent the trial error (E) as

$$E = \sum_{i=1}^{8} e_i. \tag{14}$$

The difficulty index of the task is defined based on the task bandwidth (Salvendy, 1987; Sheridan, 1992) as

$$I_d = \log_2\left(\frac{2 \times D}{W}\right), \tag{15}$$

where I_d is the difficulty index, D is the movement amplitude, and W is the target width as shown in Figure 6. Given the geometry used in this experiment, in which $D = 280$ mm and $W = 30$ mm, the difficulty index was calculated to be $I_d = 4.2$.

2.2.5 Human Performance Indexes. The human operator's performance was defined using two criteria, the completion time and the tracing accuracy (Slutski, 1998). The accuracy error was defined independently for each task, as discussed in Sections 2.2.2 and 2.2.3. According to Slutski, there are two standard equations to compute these performance indexes

$$I_1 = f(t_c) \cdot g(E), \tag{16}$$

$$I_2 = f(t_c) + g(E), \tag{17}$$

where I_i is the performance index, t_c is the completion time, E is the accuracy error, and f and g are functions of the completion time and the accuracy error, respectively. The functions f and g are defined in Section 2.4.

2.3 Experimental Procedure

Eight healthy subjects (three females and five males) 18–45 years old participated in the experimental protocol. Prior to the experiment, the three tasks were demonstrated to each subject followed by 20 min of practice with various task scenarios of time delays. Eleven discreet time delays with increments of 50 ms in the

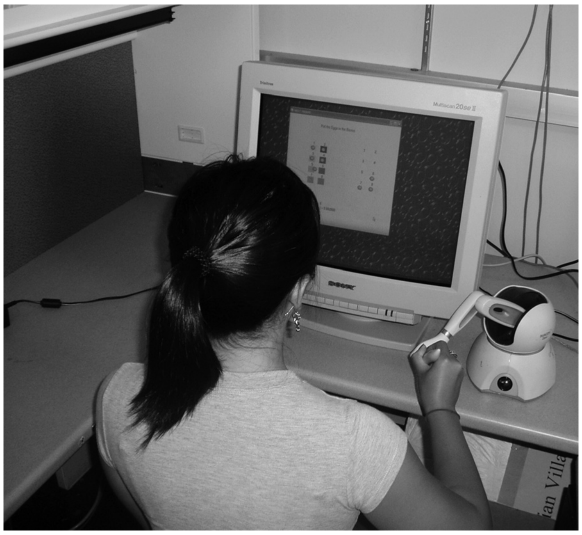

Figure 7. *Experimental setup.*

range of 0–500 ms were selected for delaying the visual picture and the force feedback independently. This resulted in 121 (11×11) different pairs of constant haptic and visual time delay values (D_H, D_V) defining the plane in Figure 2. The 121 pairs of time delay were introduced to each subject in a randomized sequence in order to eliminate adaptation and learning effects. Each subject completed 363 experiments (3 tasks $\times$ 121 experimental conditions). Each subject had two breaks of 40 min. The subjects were instructed to perform the tasks as accurately and as quickly as possible without compromising completion time over accuracy, and vice versa. Figure 7 illustrates the experimental setup.

2.4 Data Processing and Analysis-Performance Indexes

The end effector position was sampled at a rate of 1 kHz. The completion time along with the accuracy error were computed and recorded. The completion time and the error functions were defined by

$$f(t_c) = t_n, \tag{18}$$

$$t_n = t_c / t_{c(D_H = D_V = 0)}, \tag{19}$$

$$g(E) = E_n, \tag{20}$$

$$E_n = E / E_{(D_H = D_V = 0)}. \tag{21}$$

Table 2. *Average Completion Time and Accuracy Error for the Three Experimental Tasks Under No Time Delay ($D_H = D_V = 0$)*

Tasks	Average completion time, $t_{c(D_H=D_V=0)}$ (s)	Average accuracy error, $E_{(D_H=D_V=0)}$
Square tracing	8.3	16.90 cm^2
Circle tracing	5.7	12.92 cm^2
Pick and place	20.5	24 mm

The completion time and the accuracy error were then normalized with respect to their values obtained under the experimental conditions where no time delays were introduced ($D_H = D_V = 0$) and are all summarized in Table 2. Thus, the performance indexes are defined by

$$I_1 = t_n \cdot E_n, \tag{22}$$

$$I_2 = t_n + E_n. \tag{23}$$

where t_n and E_n are the normalized completion time and accuracy error.

3 Results

3.1 Tracing Tasks Results

The results indicate that the human performance across all the indexes degrades as time delays increase. Figures 8(a) and 9(a) depict the trajectory variations from the nominal tracing shape [square 8(a) and circle 9(a)] for various time delays (D_H and D_V). Figures 8(b) and 9(b) depict condensed versions of the operator's performance as 3D surfaces that are functions of haptic and visual time delays (D_H and D_V). Each of the graphs in Figures 8(a) and 9(a) is represented by a point in Figures 8(b) and 9(b), respectively.

This data reduction allows the trends in data to be visualized across the entire database. The surface gradient with respect to the visual delay is greater than the surface gradient with respect to the haptic delay $\frac{\partial t_c}{\partial D_V} > \frac{\partial t_c}{\partial D_H}$ and $\frac{\partial E}{\partial D_V} > \frac{\partial E}{\partial D_H}$ >.

Table 3 summarizes numerical values for the gradients calculated by a linear model obtained from the regres-

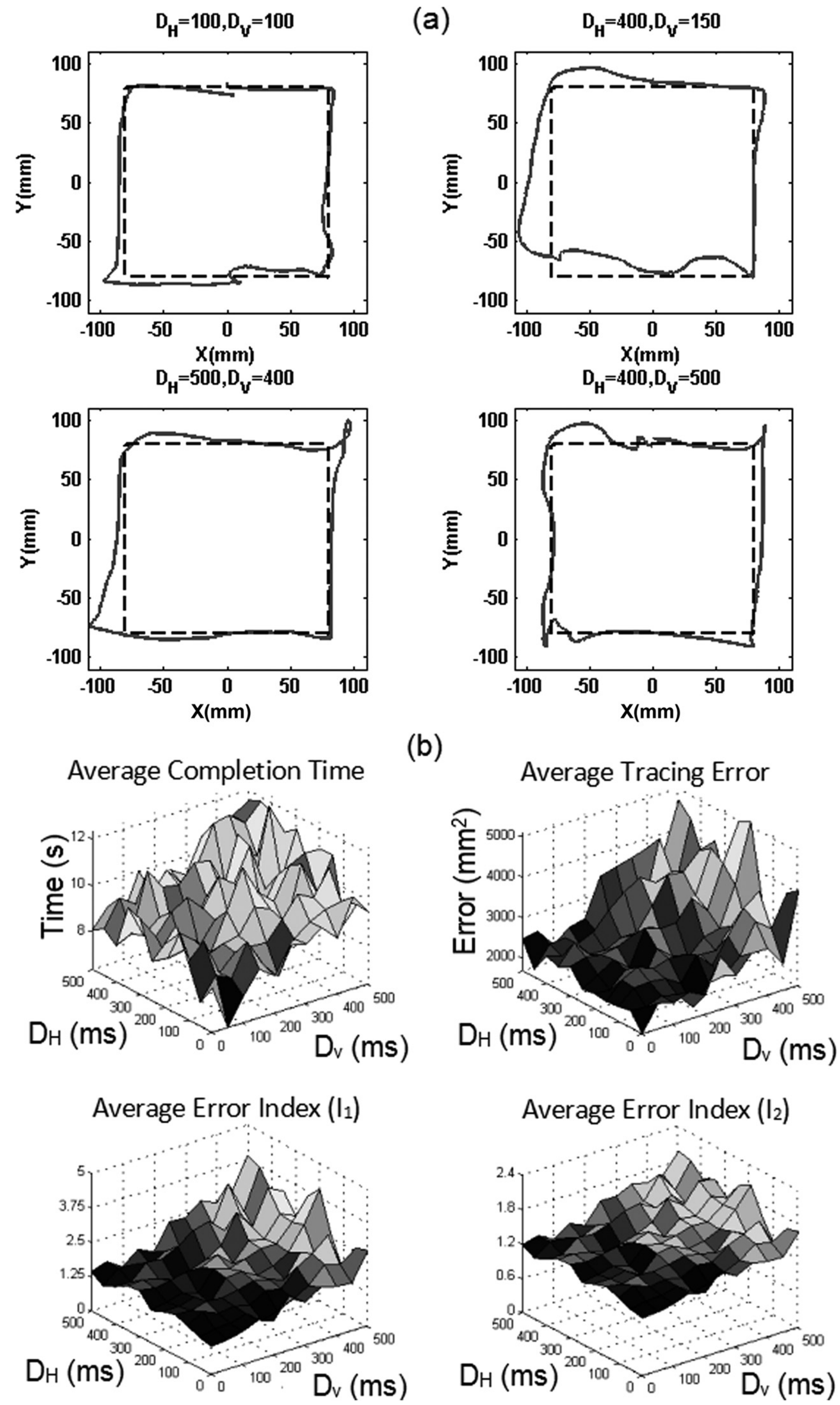

Figure 8. *Square tracing: (a) Typical square trajectories traced by various subjects with different experimental conditions of time delays (D_H and D_V) along with the normalized completion time (t_n) and tracking errors (E_n). Top left: $D_H = 100$ ms, $D_V = 100$ ms, $t_n = 0.96$, $E_n = 1.33$. Top right: $D_H = 400$ ms, $D_V = 150$ ms, $t_n = 1.3$, $E_n = 1.42$. Bottom left: $D_H = 500$ ms, $D_V = 400$ ms, $t_n = 1.25$, $E_n = 2.06$. Bottom right: $D_H = 400$ ms, $D_V = 500$ ms, $t_n = 1.4$, $E_n = 1.97$. (b) Average of subjects' performance normalized indexes.*

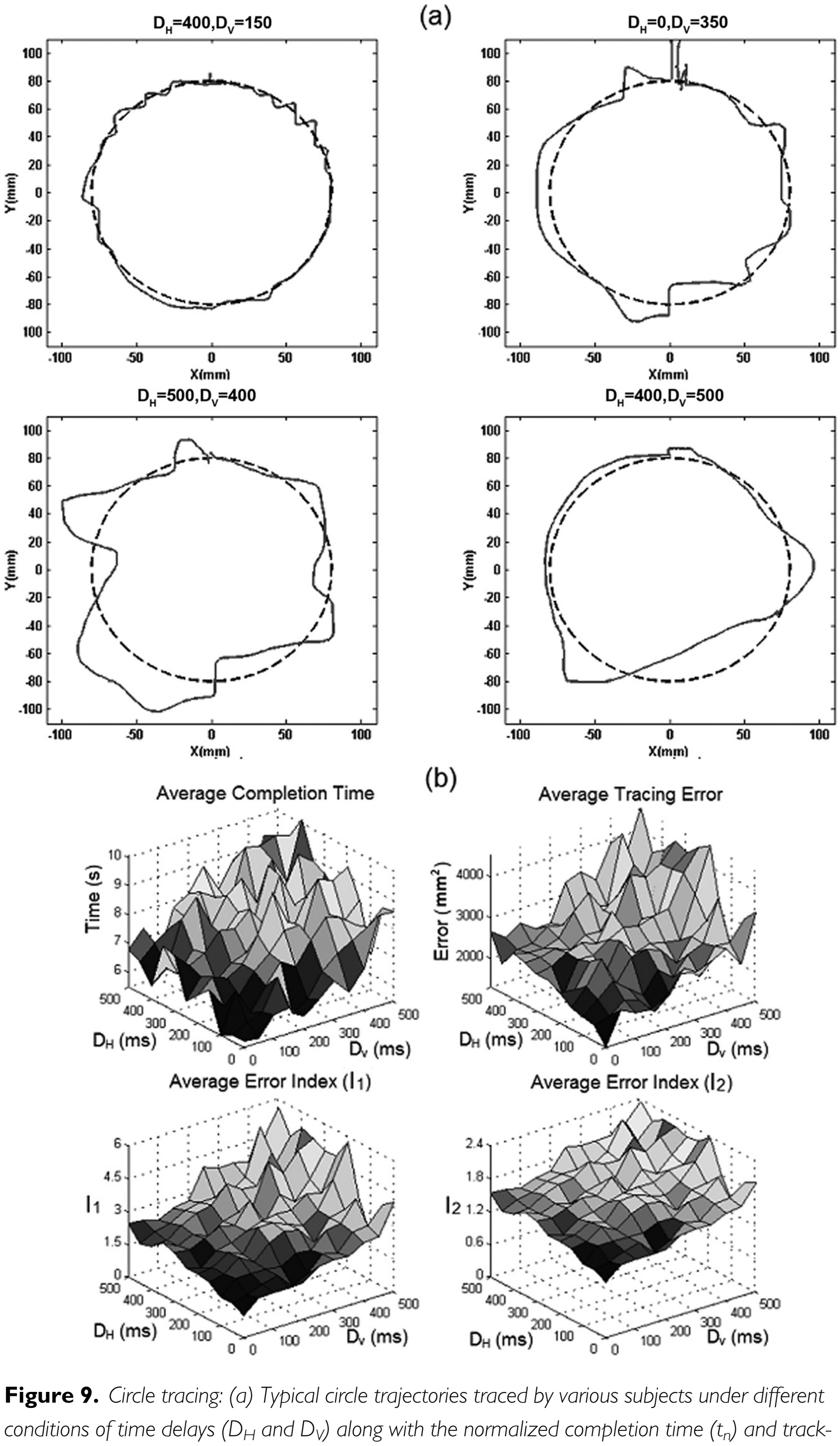

Figure 9. *Circle tracing: (a) Typical circle trajectories traced by various subjects under different conditions of time delays (D_H and D_V) along with the normalized completion time (t_n) and tracking errors (E_n). Top left: $D_H = 400$ ms, $D_V = 150$ ms, $t_n = 1.5$, $E_n = 1.88$. Top right: $D_H = 0$ ms, $D_V = 350$ ms, $t_n = 1.1$, $E_n = 2.01$. Bottom left: $D_H = 500$ ms, $D_V = 400$ ms, $t_n = 1.18$, $E_n = 3.01$. Bottom right: $D_H = 400$ ms, $D_V = 500$ ms, $t_n = 1.87$, $E_n = 2.93$. (b) Average of subjects' performance normalized indexes.*

Table 3. *Human Performance Gradients Using a Linear Model*

Performances measure	Parameters	Square tracing	Circle tracing
Completion time	$\frac{\partial t_c}{\partial D_V}$	4.418×10^{-3}	4.4724×10^{-3}
	$\frac{\partial t_c}{\partial D_H}$	2.161×10^{-3}	2.6318×10^{-3}
Accuracy error	$\frac{\partial E}{\partial D_V}$	3.175	2.841
	$\frac{\partial E}{\partial D_H}$	9.971×10^{-1}	1.615

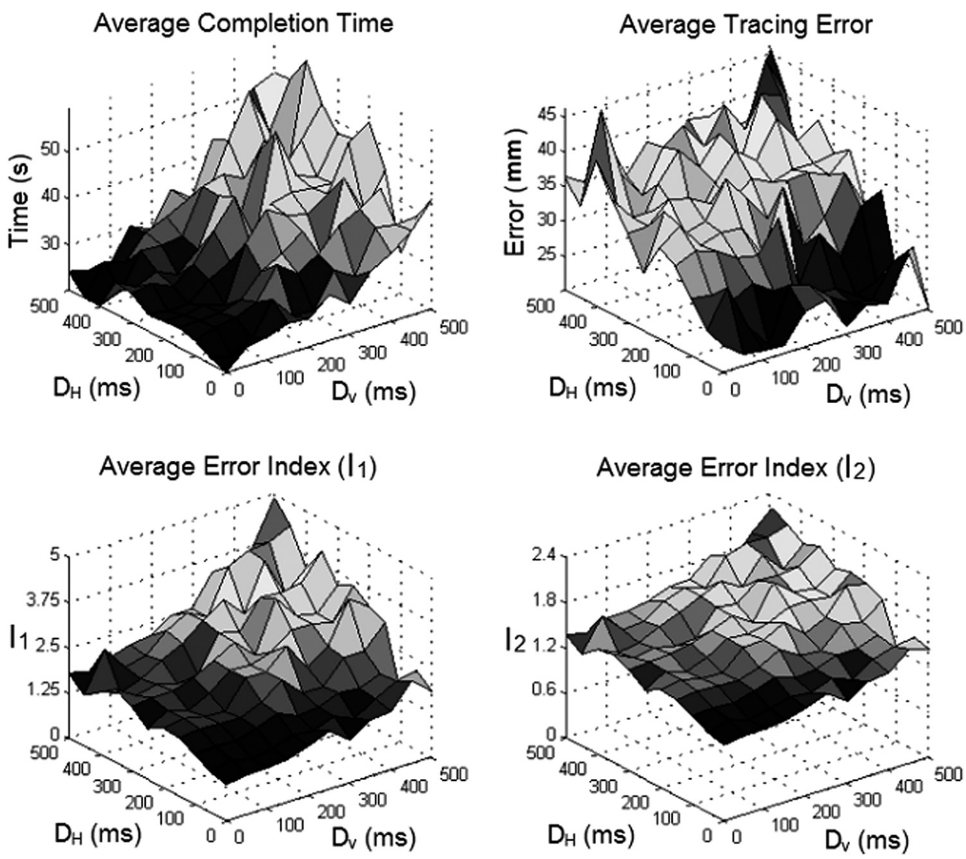

Figure 10. *Pick-and-place task—Average of the subjects' normalized performance indexes.*

sion analysis for the subjects' averages. The average error indexes (I_1, I_2) defined by Equations 22 and 23 are shown in Figures 8(b) and 9(b). The results indicate that the gradient of the second performance index (I_2) is smaller than the gradient of the first index (I_1) which gives smoother surfaces.

3.2 Pick-and-Place Task Results

The pick-and-place task provides the clearest trend and the largest gradients. The results indicate that the completion time varies within 20 s, and the placing error varies within 25 mm. Figure 10 shows both variations.

Table 4. *Statistical Significance Summary p(>|F|); Plus Sign Indicates Significant Difference; Numerical Value of Actual Probability Is Denoted*

	Square tracing		Circle tracing		Pick and place	
Performance	Haptic time delay	Visual time delay	Haptic time delay	Visual time delay	Haptic time delay	Visual time delay
Completion time	$+\ 2.3 \times 10^{-5}$	+ 8.6e-12	$+\ 3.0 \times 10^{-8}$	+ 0	$+\ 1.2 \times 10^{-3}$	+ 0
Accuracy error	$+\ 3.9 \times 10^{-3}$	+ 0	$+\ 9.3 \times 10^{-9}$	+ 0	+ 0	– 0.3473
I_1	$+\ 1.2 \times 10^{-3}$	+ 0	$+\ 6.3 \times 10^{-11}$	+ 0	+ 0	+ 0
I_2	$+\ 4.5 \times 10^{-4}$	+ 0	$+\ 5.8 \times 10^{-13}$	+ 0	+ 0	+ 0

The completion time highly depends on the visual feedback delay and is less affected by the haptic feedback delay while the accuracy error case is reversed. The visual delay has insignificant effect on the error, but the error increases significantly as the haptic delay increases.

3.3 Analysis of Variance (ANOVA)

The results of a two-way analysis of variance (ANOVA) indicate for all tasks under study—with only one exception—that the null hypothesis (H_0) should be rejected and the alternative hypothesis (H_1) should be accepted, indicating that there is a significant difference between the performance indexes for various time delays ($p < .004$; see Table 4). The only exception is the insignificant effect of the visual time delay on the accuracy error of the pick-and-place task ($p = .347$). Appendix A contains the complete ANOVA results.

3.4 Surface Regression

A surface fit analysis is performed to express the completion time, the accuracy errors, and the error indexes as functions of the haptic and the visual time delays. Four regression models given by Equations 24–27 were tested where $\gamma_i >s$ are the model's coefficients.

$$\Upsilon = \gamma_1 \cdot D_V + \gamma_2 \cdot D_H + \gamma_3, \tag{24}$$

$$\Upsilon = \gamma_3 \cdot e^{\gamma_1 . D_V + \gamma_2 . D_H}, \tag{25}$$

$$\Upsilon = \gamma_1 \cdot D_V^2 + \gamma_2 \cdot D_H^2 + \gamma_3 \cdot D_V \cdot D_H + \gamma_4 \cdot D_V + \gamma_5 \cdot D_H + \gamma_6, \tag{26}$$

$$\Upsilon = e^{\gamma_1 \cdot D_V^2 + \gamma_2 \cdot D_H^2 + \gamma_3 \cdot D_V \cdot D_H + \gamma_4 . D_V + \gamma_5 . D_H + \gamma_6}. \tag{27}$$

The goodness of fit was measured by the coefficient of determination r^2 (Soong, 2004). Equation 28 is proposed for calculating the modified goodness of fit ($r_a^2 >$) which compensates for the fact that high order models tend to provide better estimation (Soong).

$$r_a^2 = 1 - \frac{n-1}{n-k-1}(1 - r^2), \tag{28}$$

where r^2 is the goodness of fit, n is the number of readings, which equals 121, and k is the number of terms in the model. Table 5 lists the values of $r_a^2 >$ for the different models. The results summarized in Table 5 indicate that the best model under study that fits the data was a second order exponential model as in Equation 27. This model tends to better fit the data collected in the pick-and-place task compared to the tracing tasks. The models' coefficients will be referred to by the models' parameters and are listed, for each equation, in Table 6.

4 Conclusions and Discussion

In general, the results indicate that human performance in teleoperation degrades as the visual and haptic feedback information is delayed. The two-way ANOVA analysis shows a significant difference in performance degradation across the two types of time delays. In the tracing tasks (square and circle), the effect of the visual time delay is greater than the effect of the haptic time delay on the performance degradation.

The trajectories of the square tracing task indicate that the largest error occurs at the corners when a rapid

Table 5. *Modified Coefficient of Determination (r_a^2) for Various Models*

Criterion	Task	Equation 24	Equation 25	Equation 26	Equation 27
Completion time	Square tracing	0.470051	0.467487	0.495789	0.488737
	Circle tracing	0.614564	0.61641	0.615579	0.625053
	Pick and place	0.760205	0.791692	0.794421	0.813263
Accuracy error	Square tracing	0.582667	0.611897	0.628947	0.633263
	Circle tracing	0.637949	0.66359	0.667579	0.673158
	Pick and place	0.664513	0.663077	0.707789	0.723158
I_1	Square tracing	0.647385	0.692821	0.711579	0.720316
	Circle tracing	0.725333	0.774051	0.756842	0.783368
	Pick and place	0.744103	0.783487	0.837579	0.846421
I_2	Square tracing	0.670974	0.689641	0.718947	0.720316
	Circle tracing	0.761128	0.777744	0.777474	0.787263
	Pick and place	0.77559	0.787282	0.841263	0.842316

change in the trajectory line takes place as shown in Figure 8(a). As the subject traces the square edge, the magnitude of the haptic feedback is distorted due to time delay; however, around the corners, both the magnitude and the direction change rapidly, and lead to relatively larger overall tracing error. On the other hand, in tracing the circle, both the direction and the magnitude of the haptic feedback change constantly as shown in Figure 9(a); this may explain the larger tracing errors and longer completion time as the two time delays increased.

In the pick-and-place task, the completion time is mainly affected by the visual time delay, whereas the accuracy error is affected by the haptic time delay. Since moving the objects takes the majority of the time, any visual time delay slows the overall performance. In that respect, the subjects relied completely on the visual feedback in order to complete this portion of the task. The haptic feedback was used by the subjects as a guiding mechanism to position the objects accurately in their final destination; therefore, the haptic delay directly affected the accuracy performance. Consequently, we may conclude that in tracing tasks, the haptic and the visual feedback are both utilized simultaneously to optimize the performance; however, in tasks similar to the pick and place, each of the visual feedback and the force feedback is used for a different segment of the task. The results support the notion that the shape and the magnitude of the effect that the visual and the haptic time delays have on performance are related to the geometry and the segments of action involved in the task.

The following postprocessing analysis was done in order to study the effects of the hybrid performance indexes I_1 and I_2, as defined by Equations 22 and 23, on the reported data. Assuming that the completion time and accuracy are ranked on a scale from 1 to 10 such that a value of 1 represents the best performance (short completion time—high speed; and small tracking error—accuracy) and 10 represents the worst performance (long completion time—slow speed; and high tracking error—inaccuracy). The two scales are in the range of 1–10 and will be mapped into a range from 1 to 100 by performance index I_1 and from 2 to 20 by performance index I_2. In order to explore the nature of the two performance indexes several cases are presented and summarized in Table 7. In general, performance index I_1 rewards subjects that tend to excel in only one performance parameter (Subject 1, 9%; or Subject 2, 9%), more than those that make the trade-off between speed and accuracy (Subject 3, 25%), so midrange performance is not rewarded. However index I_2 gives equal evaluation to subjects who excel in one performance parameter (Subject 1, 50%; or Subject 2, 50%) as well as to subjects with midrange performance (Subject 3, 50%). Indexes I_1 and I_2 give a close score for subjects

Table 6. *Model Parameters (Equations 27 and 24) for Various Tasks and Performance Criteria; Note that Model Represents a Factor of Performance Degradation with Respect to the Nominal Experimental Condition Where Time Delays Were Set to Zero (No Time Delay); ST, CT, and PP Stand for Square Tracing, Circle Tracing, and Pick-and-Place, Respectively*

Model type		Exponential regression model (Equation 27)						Linear regression model (Equation 24)		
Criterion	Task	γ_1	γ_2	γ_3	γ_4	γ_5	γ_6	γ_1	γ_2	γ_3
Completion time	ST	4.49×10^{-7}	-8.4×10^{-7}	-8.4×10^{-7}	1.84×10^{-4}	5.9×10^{-4}	2.06	4.42×10^{-3}	2.16×10^{-3}	7.77
	CT	-3.8×10^{-7}	-7.3×10^{-7}	-1.5×10^{-7}	8.3×10^{-4}	7.6×10^{-4}	1.714	4.47×10^{-3}	2.63×10^{-3}	5.72
	PP	-1.2×10^{-7}	-1.35×10^{-6}	1.14×10^{-6}	1.2×10^{-3}	6.92×10^{-4}	3.067	0.04791	1.14×10^{-3}	18.83
Accuracy error	ST	1.6×10^{-6}	-5×10^{-7}	6×10^{-7}	1.44×10^{-4}	4.54×10^{-4}	7.622	3.175	9.97×10^{-1}	1736
	CT	9×10^{-7}	-1×10^{-6}	0	5.53×10^{-4}	1.135×10^{-3}	7.437	2.841	1.615	1533
	PP	5.7×10^{-6}	-2×10^{-6}	8.77×10^{-7}	-4.68×10^{-4}	1.765×10^{-3}	3.19071	2.03×10^{-3}	0.03095	23.81
I_1	ST	2.04×10^{-6}	-1.3×10^{-6}	8×10^{-7}	3.28×10^{-4}	1.044×10^{-3}	0.1386	3.1×10^{-3}	1.13×10^{-3}	0.846
	CT	5.62×10^{-7}	-1.8×10^{-6}	-1.1×10^{-7}	1.38×10^{-3}	1.9×10^{-3}	0.251	4.6×10^{-3}	2.6×10^{-3}	0.97
	PP	4.52×10^{-7}	-3.3×10^{-6}	2×10^{-6}	7.27×10^{-4}	2.46×10^{-3}	0.0547	3.4×10^{-3}	0.002846	0.65
I_2	ST	1.1×10^{-6}	-6.7×10^{-7}	4.2×10^{-7}	1.26×10^{-4}	5.194×10^{-4}	0.0591	1.1×10^{-3}	3.96×10^{-4}	0.98
	CT	3.35×10^{-7}	-8.74×10^{-7}	-2.1×10^{-9}	6.57×10^{-4}	9.3×10^{-4}	0.1097	1.34×10^{-3}	7.72×10^{-4}	1.078
	PP	4.47×10^{-7}	-1.6×10^{-6}	7.83×10^{-7}	3.04×10^{-4}	1.27×10^{-3}	0.0293	1.1×10^{-3}	9.57×10^{-4}	0.957

Table 7. *Analysis of Performance Indexes I_1 and I_2*

Subject number	Speed	Accuracy	Index I_1 (1–100)		Index I_2 (2–20)	
1	1	9	9	9%	10	50%
2	9	1	9	9%	10	50%
3	5	5	25	25%	10	50%
4	1	1	1	1%	2	10%
5	9	9	81	81%	18	90%

who have weak results on both performance measures (Subject 5 performed slowly and inaccurately, had an 81% score on I_1 and 90% on I_2). Using the scales differently (for example, 10 means the best while 1 means the worst) gives a different meaning for the indexes evaluations. This note is important when trying to understand the overall performance of a subject using the defined indexes.

Since the experimental protocol was defined in the context of a surgical procedure, it is possible to expand the discussion regarding the effect of completion time versus accuracy in that context. The ultimate performance measure in surgery is the clinical outcome. The outcome is affected by many factors, including but not limited to the motor skills of the surgeons and the surgical telerobotic system performance. Major aspects such as the quality and the timing of the decision-making process, as well as the proficiency of the anesthesiologists and nurses, may directly affect the clinical outcome. However, as far as speed and accuracy are concerned, they should both be maximized to guarantee the expected clinical outcome. Moreover, speed and accuracy are commonly used in surgery and other teleoperation studies due to the fact that they are qualitative parameters that are relatively easy to measure. Describing the process associated with surgery that is based on task decomposition provided deeper understanding and better skill assessment parameters to objectively assess the manual skills (Rosen et al., 2002, 2003, 2006).

Examining the various regression models (Equations 24–27) indicated that the best fit was given by the second-order exponential function (Equation 27) according to the modified coefficient of determination r_a^2 with values between 0.62 and 0.84 (excluding the completion

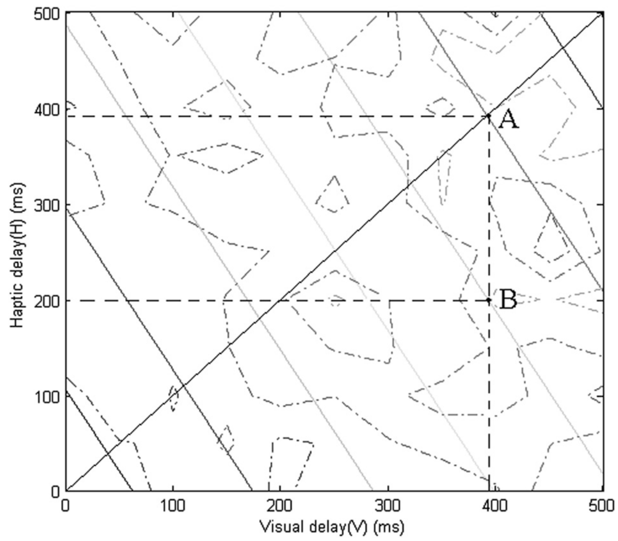

Figure 11. *Isoperformance lines of the circle tracing completion time. The dotted lines are the originals and the solid lines are the estimated contours from regression.*

time criteria of the square tracking); see Table 5. Given the same exclusion, a linear regression provided values of r_a^2 between 0.61 and 0.77 (Equation 24) and therefore may offer a simpler predictive model. Using a linear regression model, isoperformance contours can be depicted as straight lines, as shown in Figure 11.

In practice, the visual time delay is larger than the haptic time delay, since the amount of information that is transmitted across the network is larger for a video signal compared to the haptic signal. Moreover, the time that is needed to compress the video in the remote site and to decompress it locally is added to the time delay of the network. Consequently, realistic teleoperation conditions mostly occupy the feel-first-see-later region (Figure 2) of the time delay domain where $D_H > D_V$

(point B in Figure 11). Given these circumstances, one of the questions that may be raised is whether synchronizing the two delays by deliberately increasing the haptic time delay may improve human performance. Synchronizing the visual and haptic time delays will move the operation point B in Figure 11 to its new location at point A along the diagonal line of the delay space on which the two time delays are equal. At point A, the user sees and feels the teleoperated object in the remote location at the same moment. The results indicate that human performance is worse at point A than at point B. Consequently, synchronizing the two delays may degrade the performance, and keeping the two time delays nonsynchronized leads to better human performance. This result agrees in part with previously published results (Jay & Hubbold, 2005) indicating that the human performance under a combination of equal visual and haptic time delays is worse than the human performance that results when either the visual or the haptic information is delayed.

The underplaying assumption of this study is that the time delays are constant and fixed in time. In real teleoperation conditions, the time delay (visual and haptic) has a specific distribution that may change in time (mean and variance) if the user does not have control over the traffic of the network. This scenario presents even more challenging operational conditions since that operator needs to change the teleportation strategy as he or she tries to adapt to the changing characteristics of the network. Under the assumptions made in this study, the results suggest that increasing any one of the two time delays given an operational point of a specific combination of two time delays will lead to a further degradation of human performance.

References

Anderson, R. J., & Spong, M. W. (1989). Bilateral control of teleoperators with time delay. *IEEE Transactions on Automatic Control, 34*(5), 494–501.

Brown, J. D., Rosen, J., Chang, L., Sinanan, M. N., & Hannaford, B. (2004). Quantifying surgeon grasping mechanics in laparoscopy using the Blue DRAGON system. *Studies in Health Technology and Informatics, Medicine Meets Virtual Reality,* Vol. 98 (pp. 34–36). Amsterdam: IOS Press. doi: 10.3233/978-1-60750-942-4-34

Ferrell, W. (1965). Remote manipulation with transmission delay. *IEEE Transaction on Human Factors in Electronics, 6*(1), 24–32.

Flash, T., & Gurevich, I. (1997). Models of motor adaptation and impedance control in human arm movements. In P. Morasso and V. Sanguineti (Eds.), *Self organization, cortical maps and motor control* (pp. 423–481). Amsterdam: North-Holland.

Fried, G. M., Feldman, L. S., Vassiliou, M. C., Fraser, S. A., Stanbridge, D., Ghitulescu, G., & Andrew, C. G. (2004). Proving the value of simulation in laparoscopic surgery. *Annals of Surgery, 240*(3), 518–528.

Hannaford, B. (1989). Design framework for tele-operators with kinesthetic feedback. *IEEE Transactions on Robotics and Automation, 5*(4), 426–434.

Harnett, B., Doarn, C., Rosen, J., Hannaford, B., & Broderick, T. (2008). Evaluation of unmanned airborne vehicles and mobile robotic telesurgery in an extreme environment. *Telemedicine and e-Health, 14*(6), 539–544.

Hashimoto, T., Sheridan T., & Noyes M. (1986). Effect of predicted information in teleoperation through a time delay. *Japanese Journal of Ergonomics, 22*(2), 91–92.

Jay, C., & Hubbold, R. J. (2005). Delayed visual and haptic feedback in a reciprocal tapping task. *Proceedings of the First Joint EuroHaptics Conference and IEEE Symposium on Haptic Interfaces for Virtual Environment and Teleoperator Systems* (pp. 655–656).

Kelley, C. R. (1968). *Manual and automatic control.* New York: Wiley.

Lum, M. J. H., Friedman, D. C. W., King, H. H. I., Donlin, R., Sankaranarayanan, G., Broderick, T. J., . . . Hannaford, B. (2007). *Teleoperation of a surgical robot via airborne wireless radio and transatlantic internet links.* Paper presented at the Sixth International Conference on Field and Service Robotics.

Lum, M. J. H., Friedman, D. C. W., Sankaranarayanan, G., King, H., Wright, A., Sinanan, M. N., . . . Hannaford, B. (2008). Objective assessment of telesurgical robot systems. *Telerobotic FLS, Medicine Meets Virtual Reality, MMVR 16,* 263-265.

Lum, M. J. H., Rosen, J., King, H., Friedman, D. C. W., Donlin, R., Sankaranarayanan, G., . . . Hannaford, B. (2007). Telesurgery via unmanned aerial vehicle (UAV) with a field deployable surgical robot. *Proceedings of Medicine Meets Virtual Reality, MMVR 15*, 313–315.

Magnusson, P. C., Alexander, G. C., Tripathi, V. K., & Raton, B. (1992). *Transmission lines and wave propagation.* Boca Raton, FL: CRC Press.

Niemeyer, G. (1996). *Using wave variables in time delayed force reflecting teleoperation* (Ph.D. dissertation). MIT, Cambridge, MA.

Peters, J. H., Fried, G. M., Swanstrom, L. L., Soper, N. J., Sillin, L. F., Schirmer, B., . . . SAGES FLS Committee. (2004). Development and validation of a comprehensive program of education and assessment of the basic fundamentals of laparoscopic surgery. *Surgery, 135*(1), 21–27.

Pfann, K. D., Corcos, D. M., Moore, C. G., & Hasan, Z. (2002). Circle-drawing movements at different speeds: Role of inertial anisotropy. *Journal of Neurophysiology, 88*(5), 2399-2407.

Rosen, J., Brown, J. D., Chang, L., Barreca, M., Sinanan, M. N., & Hannaford, B. (2002). The Blue DRAGON: A system for measuring the kinematics and the dynamics of minimally invasive surgical tools in vivo. *Proceedings of the IEEE International Conference on Robotics & Automation, ICRA,* Vol. 2, 1876–1881.

Rosen, J., Brown, J. D., Chang, L., Sinanan, M. N., & Hannaford, B. (2006). Generalized approach for modeling minimally invasive surgery as a stochastic process using a discrete Markov model. *IEEE Transactions on Biomedical Engineering, 53*(3), 399–413.

Rosen, J., Chang, L., Brown, J. D., Hannaford, B., Sinanan, M. N., & Satava, R. (2003). Minimally invasive surgery task decomposition. Etymology of endoscopic suturing. *Studies in Health Technology and Informatics, Medicine Meets Virtual Reality,* Vol. 94 (pp. 295–301). Amsterdam: IOS Press.

Rosen, J., Lum, M. J. H., Sinanan, M. N., & Hannaford, B. (2011). Raven: Developing a surgical robot from a concept to a transatlantic teleoperation experiment. In J. Rosen, B. Hannaford, & R. M. Satava (Eds.), *Surgical Robotics: Systems, Applications, and Visions.* Berlin: Springer.

Salvendy, G. (Ed.). (1987). *Handbook of human factors.* New York: Wiley-Interscience.

Sankaranarayanan, G., & Hannaford, B. (2008). Experimental internet haptic collaboration using virtual coupling schemes. *IEEE Symposium on Haptic Interfaces for Virtual Environment and Teleoperation Systems, IEEE Haptics 2008,* 259–266.

Sankaranarayanan, G., Hannaford, B., King, H., Ko, S., Lum, M. J. H., Friedman, D., & Rosen, J. (2007, Oct.). *Portable surgery master station for mobile robotic surgery.* Paper presented at ROBOCOMM, the First International Conference on Robot Communication and Coordination.

Sheridan, T. B. (1992). *Telerobotics, automation, and human supervisory control.* Cambridge, MA: MIT Press.

Sheridan, T. B., & Ferrell, W. R. (1963). Remote manipulative control with transmission delay. *IEEE Transactions on Human Factors in Electronics, 4*(1), 25–29.

Slutski, L. (1998). *Remote manipulation systems.* Norwell, MA: Kluwer Academic.

Soong, T. T. (2004). *Fundamentals of probability and statistics for engineers.* New York: John Wiley & Sons.

Stanney, K. M. (2002). *Handbook of virtual environments.* Mahwah, NJ: Lawrence Erlbaum.

Vertut, J., Micaelli, A., Marchal, P., & Guittet, J. (1981). *Short transmission delay on a force reflective bilateral manipulator.* Paper presented at the Fourth Rom-An-Sy, Warsaw.

Appendix A: ANOVA Results

Table A1. *ANOVA Results for Average Completion Time of the Tasks**

Task	Source	SS	DOF	MS	F	Pr(>|F|)
Square tracing	Columns (visual delay)	62.8128	10	6.2813	10.3431	8.6623×10^{-12}
	Rows (kinesthetic delay)	27.8307	10	2.7831	4.5827	2.3682×10^{-5}
	Error	60.7292	100	0.6073	—	—
	Total	151.3727	120	—	—	—
Circle tracing	Columns (visual delay)	62.0232	10	6.2023	15.4017	2.2204×10^{-16}
	Rows (kinesthetic delay)	28.2124	10	2.8212	7.0058	3.0167×10^{-8}
	Error	40.2703	100	0.4027	—	—
	Total	130.5060	120	—	—	—
Pick and place	Columns (visual delay)	7.1258×10^{3}	10	712.5772	38.5494	0
	Rows (kinesthetic delay)	596.1224	10	59.6122	3.2249	0.0012
	Error	1.8485×10^{3}	100	18.4848	—	—
	Total	9.5704×10^{3}	120	—	—	—

*Note: DOF: degree of freedom, SS: sum of squares, MS: SS/df.

Table A2. *ANOVA Results for Average Tracking Error of the Tasks**

Task	Source	SS	DOF	MS	F	Pr(>|F|)
Square tracing	Columns (visual delay)	3.4299×10^{7}	10	3.4299×10^{6}	19.8365	0
	Rows (kinesthetic delay)	4.8941×10^{6}	10	4.8941×10^{5}	2.8304	0.0039
	Error	1.7291×10^{7}	100	1.7291×10^{5}	—	—
	Total	5.6484×10^{7}	120	—	—	—
Circle tracing	Columns (visual delay)	2.7115×10^{7}	10	2.7115×10^{6}	20.7348	0
	Rows (kinesthetic delay)	9.7523×10^{6}	10	9.7523×10^{5}	7.4574	9.3371×10^{-9}
	Error	1.3077×10^{7}	100	1.3077×10^{5}	—	—
	Total	4.9945×10^{7}	120	—	—	—
Pick and place	Columns (visual delay)	119.2623	10	11.9262	1.1306	0.3473
	Rows (kinesthetic delay)	3.1496×10^{3}	10	314.9603	29.8590	0
	Error	1.0548×10^{3}	100	10.5483	—	—
	Total	4.3237×10^{3}	120	—	—	—

*Note: DOF: degree of freedom, SS: sum of squares, MS: SS/df.

Table A3. *ANOVA Results for the First Error Index* I_1*

Task	Source	SS	DOF	MS	F	Pr(>|F|)
Square tracing	Columns (visual delay)	32.1868	10	3.2187	23.5178	0
	Rows (kinesthetic delay)	4.4260	10	0.4426	3.2339	0.0012
	Error	13.6861	100	0.1369	—	—
	Total	50.2989	120	—	—	—
Circle tracing	Columns (visual delay)	68.7358	10	6.8736	29.1303	0
	Rows (kinesthetic delay)	22.3691	10	2.2369	9.4800	6.3979×10^{-11}
	Error	23.5960	100	0.2360	—	—
	Total	114.7009	120	—	—	—
Pick and place	Columns (visual delay)	35.6749	10	3.5675	23.1880	0
	Rows (kinesthetic delay)	27.2490	10	2.7249	17.7113	0
	Error	15.3851	100	0.1539	—	—
	Total	78.3090	120	—	—	—

*Note: DOF: degree of freedom, SS: sum of squares, MS: SS/df.

Table A4. *ANOVA Results for the Second Error Index* I_2*

Task	Source	SS	DOF	MS	F	Pr(>|F|)
Square tracing	Columns (visual delay)	3.8432	10	0.3843	24.9226	0
	Rows (kinesthetic delay)	0.5501	10	0.0550	3.5671	4.5204×10^{-4}
	Error	1.5421	100	0.0154	—	—
	Total	5.9353	120	—	—	—
Circle tracing	Columns (visual delay)	5.6984	10	0.5698	32.7954	0
	Rows (kinesthetic delay)	2.0083	10	0.2008	11.5580	5.8431×10^{-13}
	Error	1.7376	100	0.0174	—	—
	Total	9.4442	120	—	—	—
Pick and place	Columns (visual delay)	3.7566	10	0.3757	29.3759	0
	Rows (kinesthetic delay)	3.1267	10	0.3127	24.4506	0
	Error	1.2788	100	0.0128	—	—
	Total	8.1621	120	—	—	—

*Note: DOF: degree of freedom, SS: sum of squares, MS: SS/df.